Emergence and Control of Complex Behaviours in Driven Systems of Interacting Qubits with Dissipation. SUPPLEMENTARY MATERIALS.

A. V. Andreev[1], A. G. Balanov[2,+], T. M. Fromhold[3], M. T. Greenaway[2], A. E. Hramov[1], W. Li[3], V. V. Makarov[1], A. M. Zagoskin[2,4,*]

[1]*Innopolis University, Universitetskaya Str. 1, Innopolis, 420500, Russia*

[2]*Department of Physics, Loughborough University, Loughborough LE11 3TU, United Kingdom*

[3]*School of Physics and Astronomy, University of Nottingham, Nottingham NG7 2RD, United Kingdom*

[4]*Department of Theoretical Physics and Quantum Technologies, National University of Science and Technology MISIS, 4 Leninsky Ave., Moscow 119049, Russia*

[*]*Corresponding author: a.zagoskin@lboro.ac.uk and*

[+]*Corresponding author: a.balanov@lboro.ac.uk*

A. Model of electromagnetically driven interacting qubits with decoherence and dissipation

The standard description of a set of interacting qubits is provided by the Ising Hamiltonian,

$$H = \sum_j H_j + \sum_{j<k} U_{jk}, \tag{1}$$

with

$$H_j = -\frac{1}{2}\left[\epsilon_j \sigma_j^z + \delta_j \sigma_j^x\right], \quad U_{jk} = J_{jk}\sigma_j^z\sigma_k^z. \tag{2}$$

Here the Pauli operators, σ_j^α, describe the transitions between qubit states, ϵ_j and δ_j are, respectively, the bias and the tunneling matrix element in the jth qubit, and J_{jk} is the qubit-qubit coupling. In the case of superconducting qubits of various kinds all these parameters can, in principle, be tuned in experiments (see, e.g., [1, 2]). Moreover, since certain degree of control is possible for all types of currently available qubits, including Rydberg atom-based, the model (1,2) is generic. Expressing the Pauli matrices in terms of projectors to the ground and excited states of the qubits, $|g\rangle, |e\rangle$,

$$\begin{aligned} \sigma_j^z &\equiv |g\rangle\langle g|_j - |e\rangle\langle e|_j \equiv \hat{1}_j - 2|e\rangle\langle e|_j; \\ \sigma_j^x &\equiv |e\rangle\langle g|_j + |g\rangle\langle e|_j; \hat{1}_j \equiv |g\rangle\langle g|_j + |e\rangle\langle e|_j, \end{aligned} \tag{3}$$

we can rewrite (2) as

$$\begin{aligned} H_j &= -\frac{1}{2}\epsilon_j \hat{1}_j + \epsilon_j |e\rangle\langle e|_j - \frac{1}{2}\delta_j\left[|e\rangle\langle g|_j + |g\rangle\langle e|_j\right], \\ U_{jk} &= J_{jk}\left[\hat{1}_j - 2|e\rangle\langle e|_j\right] \otimes \left[\hat{1}_k - 2|e\rangle\langle e|_k\right]. \end{aligned} \tag{4}$$

This yields the Hamiltonian (1) in the form

$$H = \sum_j \left\{ \left[\epsilon_j - 2\sum_k J_{jk}\right] |e\rangle\langle e|_j - \frac{1}{2}\delta_j\left[|e\rangle\langle g|_j + |g\rangle\langle e|_j\right] \right\} + 4\sum_{jk} J_{jk}|e\rangle\langle e|_j \otimes |e\rangle\langle e|_k + \left[-\frac{1}{2}\sum_j \epsilon_j + \sum_{jk} J_{jk}\right].$$

Up to the irrelevant total energy shift, $\Delta E = \left[-\frac{1}{2}\sum_j \epsilon_j + \sum_{jk} J_{jk}\right]$, and parameter relabeling, this Hamiltonian is an inhomogeneous version of the interaction-representation Hamiltonian of a system of Rydberg atoms in a laser field [3, 4]. In the mapping of (4) on Eq.(1), δ_ω corresponds to $(\epsilon_j - 2\sum_k J_{jk})$, i.e., the role of detuning is played by the negative of the mean-field excitation energy of a qubit. The role of the Rabi frequency is, quite naturally, taken over by (the negative of) the matrix element of interlevel transition, $-\delta_j$. The interqubit couplings J_{jk} map to the factor $V/8(N-1)$ in Eq.(1). As mentioned above, for the exact analogy with Rydberg atoms we must assume that there is no dispersion of qubit properties, but such an assumption is not necessary when investigating the qubit dynamics.

The evolution for one-qubit density matrix ρ_j is obtained directly from the von Neumann equation,

$$\frac{d}{dt}\prod_j \rho_j = \frac{1}{i}[H, \prod_j \rho_j] + \mathcal{L}[\prod_j \rho_j],$$

by tracing out all qubits except the jth one. In terms of Pauli matrices (denoting the unit matrix by σ_0) and a one-qubit density matrix is expressed through the population inversion and coherence as as $\rho_j = (1/2)(\sigma_j^0 - w_j\sigma_j^z + 2\Re q_j \sigma_j^x + 2\Im q_j \sigma_j^y)$. Therefore tracing out $(N-1)$ qubits with $k \neq j$ leaves in the von Neumann equation only terms linear in $\dot{w}_j, \dot{q}_j, w_j, q_j$, plus a nonlinear term originating from the interqubit zz-coupling in Eq.(2). This term produces an effective mean-field correction to detuning. Gathering the coefficients at $\sigma_j^{x,y,z}$, we obtain Eqs.(4) in the main text.

The dynamics of the system described by Eqs. (4) in the main text was first studied in [3] for the case of Rydberg atoms with laser driving and spontaneous emission. The authors of that work investigated the transition between the uniform and antiferromagnetic phases induced by variation of the controling parameters of the system. In particular, they discovered the existence of a novel oscillatory phase and bistability between the uniform and antiferromagnetic phases. Here we focus on the detailed

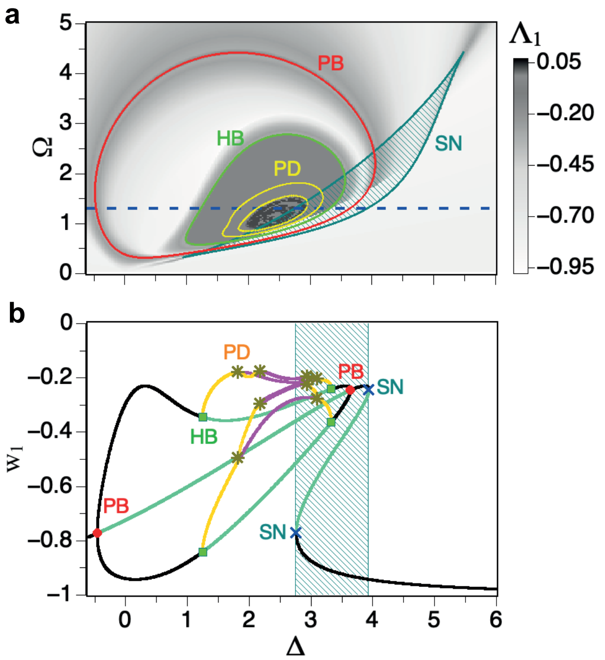

SUPPLEMENTARY FIGURE 1: (Color online) **a** Two-parametric bifurcation diagram calculated for $c = 5$. Red curve (PB), green curve (HB), yellow curves (PD) and dark-green curve (SN) are loci of pitch-fork, Andronov-Hopf, period-doubling and saddle-node bifurcations, respectively. The gray scale intensity indicates the value of the largest Lyapunov exponent Λ_1. **b** Single-parametric bifurcation diagram along the blue dashed line in **a** for $\Omega = 1.3$. Black and green points correspond to stable and unstable fixed points, respectively; brown/magenta points indicate the maximal value of w_1 corresponding to stable/unstable periodic oscillations. The red circles (PB), green squares (HB), dark-yellow asterisks (PD) and blue crosses (SN) denote pitchfork, Hopf, period-doubling and saddle-node bifurcation, respectively. In both **a** and **b** the cross-hatched area marks the region of multistability, where a homogeneous fixed point coexists with other solutions.

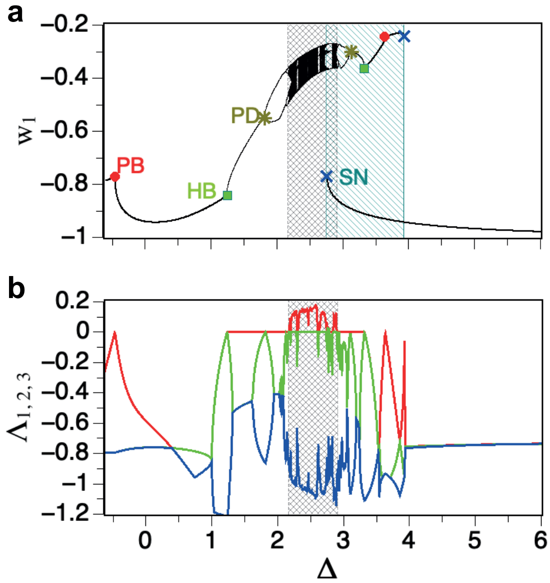

SUPPLEMENTARY FIGURE 2: (Color online) Single-parametric bifurcation diagram illustrating evolution of stable regimes with variation of Δ. The black dots correspond to the Poincaré section $\dot{w}_1 + \dot{w}_2 = 0$. **b** Dependence of the three largest Lyapunov exponents $\Lambda_{1,2,3}$ on Δ. Both **a** and **b** were calculated for $c = 5$ and $\Omega = 1.3$, along the blue dashed line in Suppl. Fig. 1a. The shaded area in **a** marks the region of multistability, cross-hatched areas [in both **a** and **b**] denote the chaos region.

bifurcation analysis of multiple coupled qubits systems and on the transitions to the chaotic dynamics found in our investigation.

B. Dynamics of two qubits

The results of our analysis for two qubits are summarized in Suppl. Fig. 1a , where the bifurcation diagram in the parameter plane (Δ, Ω) is presented for the coupling parameter $c = 5$ defined in Eqs. (4) in the main text. The red line labeled PB indicates the pitchfork bifurcation, which is associated with the appearance/disappearance of two stable symmetric fixed points (steady states). The green (HB) line corresponds to the onset of the Hopf bifurcation, where stable periodic oscillations emerge/vanish in the system. The yellow curves (PD) mark the position of period-doubling bifurcations of the periodic oscillations. The dark-cyan curve (SN) shows the locus of saddle-node bifurcation, which gives birth to a pair of stable and saddle fixed points. This curve encompasses the cross-hatched area of the parameter plane, where the homogeneous fixed point, for which $w_1 = w_2$ and $q_1 = q_2$, coexists with other equilibrium or oscillatory solutions. The bifurcation lines are superimposed on a grayscale map illustrating the dependence of the largest Lyapunov exponent Λ_1 on Δ and Ω. The Lyapunov exponents were calculated for the stable limit sets, which correspond to the solutions of the model equations as time $t \to \infty$. To determine them, we utilized the theory and numerical approaches discussed in [5, 6]. The negative values of Λ_1 correspond to the fixed points (equilibrium states), zero values mean the periodic or quasiperiodic solutions, while positive Λ_1 evidences the presence of deterministic chaos [7]. A transition from white to black in Suppl. Fig. 1a reflects the change from smaller to larger values of Λ_1. The diagram clearly demonstrates the existence of chaotic dynamics ($\Lambda_1 > 0$) in considerable areas of the parameter plane shaded by dark-gray/black colors.

To better illustrate the bifurcation transitions, in

Suppl. Fig. 1b we present a single-parametric bifurcation diagram calculated for $\Omega = 1.3$, i.e. along the blue dashed horizontal line in Suppl. Fig. 1a . Each point on the diagram corresponds to the maximal value of the variable w_1 calculated for a given Δ. The black and green colors denote stable and unstable fixed points, respectively, while brown and magenta points correspond to stable and unstable periodic solutions. With Δ increasing from a negative value, the homogeneous fixed point undergoes a pitchfork bifurcation at $\Delta \approx -0.465$ (red circle labeled as PB). As a result, it becomes unstable, and in its vicinity a pair of symmetric inhomogeneous fixed points is born. Notably, it was shown in [3] that this bifurcation corresponds to phase transition between the uniform and antiferromagnetic phases. With further increase of Δ, each of these inhomogeneous (antiferromagnetic) fixed points loses its stability via the Hopf bifurcation at $\Delta \approx 1.238$ (green square HB), which leads to the appearance of stable periodic oscillations (yellow points). In turn, these oscillations become unstable due to another period-doubling bifurcation at $\Delta \approx 1.819$ (dark-yellow asterisk PD) giving birth to a stable periodic solution with doubled period. With varying Δ, these period-two oscillations undergo another period-doubling bifurcation at $\Delta \approx 2.136$ leading to the emergence of stable period-four oscillations. This sequence of period-doubling bifurcations continues with the growth of Δ, producing an infinite set of unstable periodic solutions with different periods. Eventually, this cascade of bifurcations leads to the appearance of chaotic oscillations, which are characterized by $\Lambda_1 > 0$, at $\Delta \approx 2.17$. If Δ grows even further, the bifurcation scenario discussed above develops in the opposite direction. Namely, chaos disappears through the inverse cascade of period-doubling bifurcations that starts at $\Delta \approx 2.90$. This is followed by a Hopf bifurcation ($\Delta \approx 3.322$), where the oscillations cease, and then inverse pitch-fork bifurcation ($\Delta \approx 3.636$), where symmetric ferromagnetic fixed points merge and annihilate, while the homogeneous fixed point becomes stable. The homogenous fixed points are involved in a pair of saddle-node bifurcations (blue crosses SN) at $\Delta \approx 2.756$ and $\Delta \approx 3.931$. This creates folds on the bifurcation diagram, which suggests hysteresis and forms a region of bistability (shaded area), where a homogeneous fixed point (black dots in the lower part of the diagram) coexists with other solutions (black or brown points in the upper part of the diagram).

Supplementary Figure 2a demonstrates how the stable solutions of the model equations evolve with varying Δ. The diagram exhibits the points of a Poincaré section of phase trajectories calculated for a range of Δ. We have chosen the Poincaré section defined by the equation $\dot{w}_1 + \dot{w}_2 = 0$ as it produces a diagram convenient for interpretation. Thus, for a given Δ, a single point in the bifurcation diagram represents either a fixed point or periodic oscillations of w_1. Similarly, several separated points correspond to period-added oscillations and a complex set of points reflects chaotic behavior. The bifurcation points PB, HB, PD and SN have the same interpretations as in Suppl. Fig. 1b. Since the branches of inhomogeneous solutions are symmetric with respect to swapping the state variables $\{\omega_1, q_1 \Leftrightarrow \omega_2, q_2\}$, for simplicity, Suppl. Fig. 2a shows only one branch of inhomogeneous solutions.

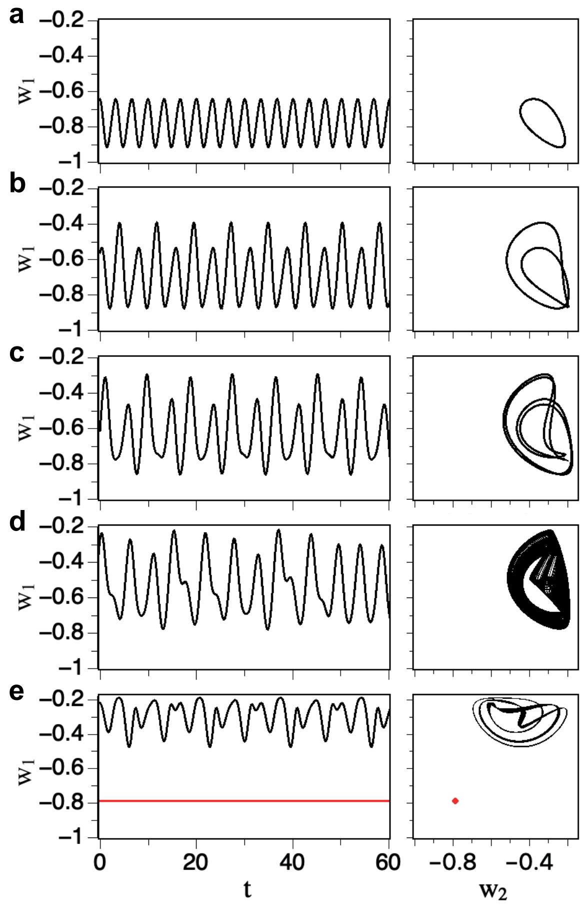

SUPPLEMENTARY FIGURE 3: Time evolution of w_1 (left panels) and the (w_1, w_2) projection of the phase trajectories (right panels) of the stable regimes calculated for $\Omega = 1.3$, $c = 5$ and **a** $\Delta = 1.5$, **b** $\Delta = 1.939$, **c** $\Delta = 2.147$, **d** $\Delta = 2.5$ and **e** $\Delta = 2.76$.

For comparison, Suppl. Fig. 2b shows the three largest Lyapunov exponents, $\Lambda_1 > \Lambda_2 > \Lambda_3$, calculated for the same range of Δ as in Suppl. Fig. 2a . One can see that in the vicinity of every bifurcation point, one of the Lyapunov exponents approaches zero thus signaling the development of instability. For small values of Δ, before the point HB, all the Lyapunov exponents are negative, which indicates that the stable regime is a steady state (fixed point). Above HB, the "period-one" stable oscillations appear in the system, which are represented in Suppl. Fig. 2a by a single point for each value of Δ. An example of such oscillations for $\Delta = 1.5$ is shown in Suppl. Fig. 3a. The left panel shows the time-domain realization of w_1, while the right panel depicts the projection of the phase trajectories of the oscillations on the (w_2, w_1) plane. The phase trajectories correspond to a limit cycle, seen as a single-loop closed curve. Period-doubling bifurcation PD destabilises period-one oscillations and gives birth to stable period-two oscillations, an example of which is shown in Suppl. Fig. 3b for $\Delta = 1.939$. The time-domain realization of this regime (left panel) shows two maxima per period, which in phase space implies a two-loop limit cycle (right panel). In Suppl. Fig. 2b the period-two limit cycle is represented by two points for each given Δ. After the second period-doubling bifurcation, the period-two oscillations lose their stability producing period-four oscillations. These oscillations are represented in Suppl. Fig. 2a by four points for a given Δ. The oscillations have four maxima per period [Suppl. Fig. 3c] and their phase trajectory forms a four-loop limit cycle. All periodic regimes are characterized by one zero Lyapunov exponent, whilst all other Lyapunov exponent are negative [see Suppl. Fig. 2b].

The evolution of period-added limit cycles with the variation of Δ leads to the appearance of deterministic chaos, whose areas of existence are cross-hatched in Figs. 2a,b. In Suppl. Fig. 2a the chaos is mapped as a complex set of points. A typical chaotic time evolution is shown in the left panel of Suppl. Fig. 3d. Although the oscillations superficially demonstrate a certain order, they are irregular, unstable, do not have any distinct period, and their phase trajectories never close; although from time to time they return to the same area of the phase space [right panel of Fig 3d]. These oscillations are characterized by one positive and one zero Lyapunov exponent, with all other Lyapunov exponents being negative. This sequence of Lyapunov exponents evidences the chaotic character of the oscillations [7]. One can see that the chaos region in Suppl. Fig. 2a is interspersed with "windows of periodicity", where the chaos is replaced by complex periodic solutions. In Suppl. Fig. 2b these windows are reflected by Λ_1 falling back to zero. The emergence of these windows of periodicity is typical for chaos born through a cascade of period-doubling bifurcations [7].

The range of Δ corresponding to bistability in the system is shown in Suppl. Fig. 2a as the cross-hatched area limited by a pair of SN points. Within this range, the homogeneous fixed point (the lower branch of the bifurcation diagram) coexists with different inhomogeneous solutions (the upper branch of the diagram). It is noteworthy that, depending on the value of Δ, the latter solution can be either another fixed point or periodic oscillations, or even chaos. An example of the coexistence of a homogeneous fixed point and chaos is shown in Suppl. Fig. 3e. The chaos in this example is weaker than that in Suppl. Fig. 3d because Λ_1 is smaller in the former. This is also reflected in the behavior of the oscillations. For instance, the phase trajectories in Suppl. Fig. 3d, forming a multi-band chaotic attractor, look more regular than the dynamics in Suppl. Fig. 3e, where the chaotic attractor demonstrates a single band with very irregular orbits.

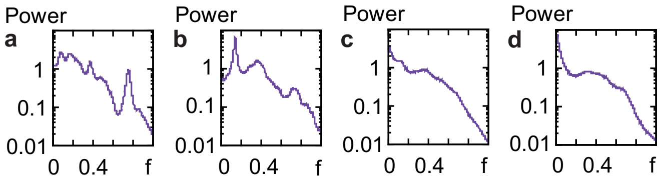

SUPPLEMENTARY FIGURE 4: Power-frequency (f) spectrum of $w_1(t)$ calculated for the dynamics of qubit chains consisting of 4 **a** , 8 **b** , 10 **c** , 20 **d** qubits for $\Omega = 2.5$, $c = 5$, $\Delta = 5.0$.

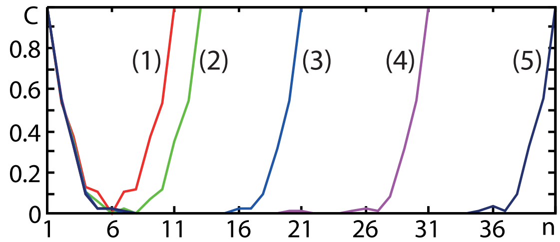

SUPPLEMENTARY FIGURE 5: Correlation coefficient, C, of the first qubit in the chain calculated versus the index, n, of the other qubit for chains with $N = 10$ (line 1), 12 (line 2), 20 (line 3), 30 (line 4) and 40 (line 5), and for $\Omega = 2.5$, $c = 5$, $\Delta = 5.0$.

C. Spectra of hyperchaotic oscillations

Figure 4 presents the power spectrum for chaotic and hyperchaotic oscillations, which emerge in the ring chains of qubits with varying N for fixed $\Omega = 2.5$, $c = 5$ and $\Delta = 5.0$. For $N = 4$ (a) the system demonstrates chaotic oscillations, which are characterized by one positive Lyapunov exponent. The chaotic oscillations demonstrate a broadband continuous spectrum with a distinct peak near the frequency $f = 0.8$ corresponding to the characteristic time scale of the oscillations. For $N = 8$ [Suppl. Fig. 4b], the oscillations existing for the parameters above become hyperchaotic with three positive Lyapunov exponents. In the Fourier spectrum, the position of the characteristic peak shifts towards lower frequency $f \approx 0.11$, which reflects the change of the character of the chaotic behavior. In addition, the peak itself becomes less pronounced as its height considerably decreases compared to the background. As N further increases (c), the distinctive characteristic peaked power spectrum disappears, and for $N > 12$ (d) the spectrum of hyperchaos varies smoothly with f, demonstrating a shape that is typical of random noise in solids, e.g. hot-electron noise in semiconductors [8].

To shed light on the dependence of the number of the positive Lyapunov exponents, M, versus N, presented in Suppl. Fig. 5, we calculated the linear correlation coefficients $c_{m,n}$, characterizing the correlations between the oscillations of the m^{th} and n^{th} qubits in the chain

$$c_{m,n} = \frac{\langle (w_m(t) - \langle w_m \rangle)(w_n(t) - \langle w_n \rangle) \rangle}{\sqrt{\langle (w_m(t) - \langle w_m \rangle)^2 \rangle \langle (w_n(t) - \langle w_n \rangle)^2 \rangle}}, \quad (5)$$

where $\langle . \rangle$ is the time average, and $m, n = 1, \ldots, N$. The n dependence of the coefficient $C = c_{1,n}$ calculated for different N is shown in Suppl. Fig. 5. Each curve is symmetric with maxima $C = 1$ for $n = 1$ and $n = N + 1$ reflecting the fact that we consider ring chains, where the first and $(N + 1)$th qubits coincide. For all N, the correlation C drops to almost zero for $n = 6$. Thus, the oscillation of the first qubit is practically unaffected by the dynamics of the 6th one. Due to this drop of correlation in chains with $N > 6$, the inclusion of a chaotic oscillator into the chain simply adds a new positive Lyapunov exponent to the spectrum. Previously, we have shown that chaotic dynamics can emerge as a cooperative phenomenon when at least two qubits interact with each other. Such interactions could provide a qualitative explanation for the almost linear dependence of M on N shown in Suppl. Fig. 5, where the inclusion of every 2-3 extra qubits into the chain with $N > 6$ produces an additional positive Lyapunov exponent for the given values of the parameters.

D. Non-identical qubits

We examined the existence of chaos and hyperchaos in chains of non-identical qubits with nearest neighbor interactions, both in ring formation and open chains, and also in a ring chain where each qubit connects with two neighbors on each side. The parameters of each qubit were detuned with a random mismatch of up to 10% of their average values: $\Delta_i = \Delta + \delta\Delta_i$, $\Omega_i = \Omega + \delta\Omega_i$, and $c_i = c + \delta c_i$. Figure 6 presents the variation of the four largest Lyapunov exponents with Δ for (a) five non-identical qubits in the ring chain, (b) ten non-identical qubits in an open chain, and (c) ten non-identical qubits in a ring chain, where each qubit interacts with two neighbors on each side. All graphs are plotted for $\Omega = 2.5$ and $c = 5$. The parameters' mismatch for the graphs in Suppl. Fig. 6a (Suppl. Fig. 6 b,c) are summarized in Suppl. Tab. I (II) respectively.

The graphs in Suppl. Fig. 6 reveal the areas of Δ that correspond to one or few positive Lyapunov exponents, i.e. areas of existence of chaos and hyperchaos, in all types of the chains considered. The latter confirms the generic character of chaos and hyperchaos phenomena in various chains of coherent quantum systems.

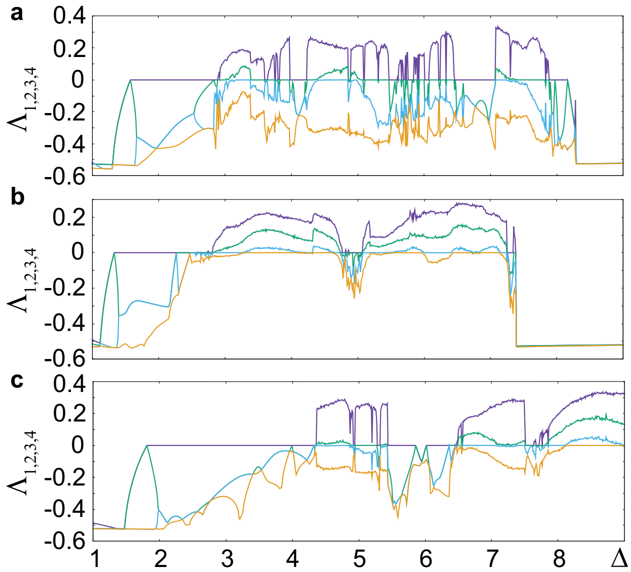

SUPPLEMENTARY FIGURE 6: Variation of the four largest Lyapunov exponents with Δ calculated for **a** five non-identical qubits in a ring chain with the parameters given in Supplementary Table I; **b** ten non-identical qubits in non-ring chain; **c** ten non-identical qubits, each connected to two nearest neighbors on each side. The parameters for **b** and **c** are summarized in Supplementary Table II; for all graphs $\Omega = 2.5$, $c = 5$.

i	$\delta\Omega_i$	$\delta\Delta_i$	δc_i
1	-0.2	$+0.45$	-0.1
2	-0.15	0	$+0.45$
3	$+0.05$	-0.4	0
4	0	-0.05	$+0.4$
5	$+0.2$	$+0.25$	-0.35

SUPPLEMENTARY TABLE I: Parameters of the five individual qubits used to calculate the graphs in Suppl. Fig. 6a, where index i labels the qubit position in the chain.

E. Entangled qubits.

To obtain insights into the role of entanglement on the dynamics of a qubit chain, we numerically integrate the von Neumann equation (Eq.(2) in the main text) for the N-particle density matrix, without any simplifying assumptions. To illustrate the results, we consider a chain of $N = 5$ qubits with nearest-neighbor interaction and calculate the average Rydberg population $\langle E \rangle (t) = \sum_j \mathrm{Tr}|e\rangle\langle e|_j/N$, where Tr denotes the trace of the density matrix. Supplementary Figure 7 shows the typical time dependence of $\langle E \rangle (t)$ calculated for fixed values of $\Delta = 2.5$, $V = 5$, $\gamma = 0.01$ and various Ω. For small $\Omega = 0.3$, the expectation value $\langle E \rangle$ demonstrates coherent, almost harmonic, oscillations (a). As Ω grows, the system transitions through quasiperiodic (b), noise-like (c), and, finally, re-entrant quasiperiodic

i	$\delta\Omega_i$	$\delta\Delta_i$	δc_i
1	-0.25	$+0.45$	-0.4
2	$+0.1$	0	$+0.15$
3	-0.15	-0.3	0
4	0	-0.1	$+0.4$
5	$+0.2$	$+0.25$	-0.2
6	-0.35	$+0.35$	-0.5
7	$+0.05$	-0.2	$+0.25$
8	-0.05	-0.35	$+0.1$
9	$+0.15$	$+0.05$	$+0.45$
10	$+0.25$	$+0.5$	-0.25

SUPPLEMENTARY TABLE II: Parameters of the ten individual qubits used to calculate the graphs in Suppl. Fig. 6b,c, where index i labels the qubit position in the chain.

decaying oscillations (d). A detailed analysis of this result, as well as investigation of the transition from the fully entangled to the factorized case in the presence of entanglement-disrupting processes, will be presented in a separate paper.

[1] Zagoskin, A. M. *Quantum engineering: theory and design of quantum coherent structures* (Cambridge University Press, 2011).

[2] Gu, X., Kockum, A. F., Miranowicz, A., Liu, Y.-x. & Nori, F. Microwave photonics with superconducting quantum circuits. *Physics Reports* **718**, 1–102 (2017).

[3] Lee, T. E., Häffner, H. & Cross, M. Antiferromagnetic phase transition in a nonequilibrium lattice of Rydberg atoms. *Physical Review A* **84**, 031402 (2011).

[4] Lee, T. E., Haeffner, H. & Cross, M. Collective quantum jumps of Rydberg atoms. *Physical Review Letters* **108**, 023602 (2012).

[5] Oseledets, V. I. A multiplicative ergodic theorem. Characteristic Ljapunov exponents of dynamical systems. *Trans. Moscow Math. Soc.* **19**, 197–231 (1968).

[6] Wolf, A., Swift, J. B., Swinney, H. L. & Vastano, J. A. Determining Lyapunov exponents from a time series. *Physica D: Nonlinear Phenomena* **16**, 285–317 (1985).

[7] Anishchenko, V. S. *Dynamical Chaos, Models and Experiments: Appearance Routes and Structure of Chaos in Simple Dynamical Systems* (World Scientific Publishing, Singapore, 1995).

[8] Kogan, S. *Electronic noise and fluctuations in solids* (Cambridge University Press, 2008).

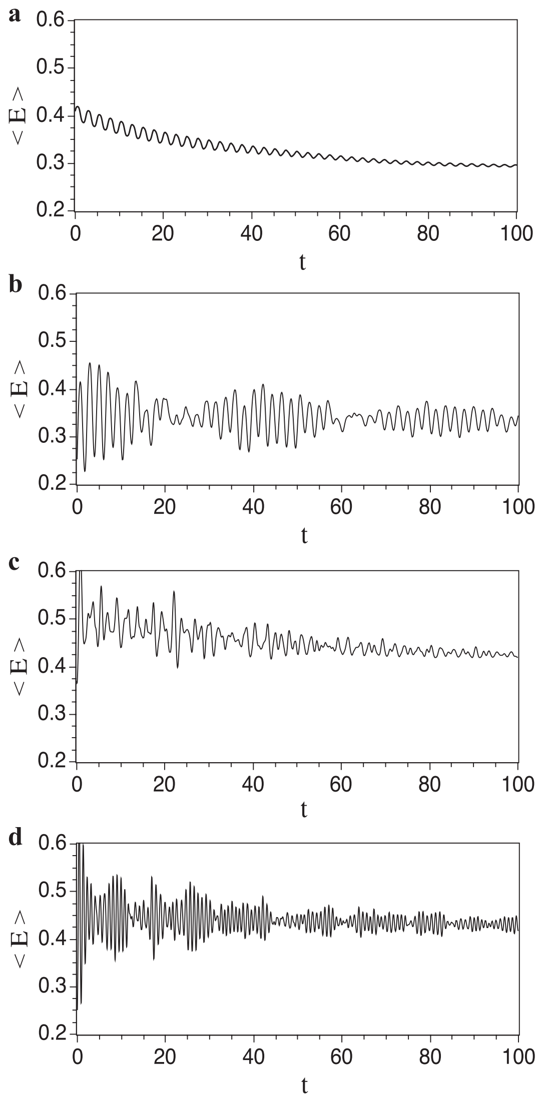

SUPPLEMENTARY FIGURE 7: Time evolution of $\langle E\rangle$ calculated for $\Delta = 2.5$, $V = 5$, $\gamma = 0.01$ and **a** $\Omega = 0.3$, **b** $\Omega = 1.3$, **c** $\Omega = 3.3$ and **d** $\Omega = 5.7$.